Appl. Phys. B 77, 455–461 (2003)
DOI: 10.1007/s00340-003-1256-x

Applied Physics B
Lasers and Optics

S. BAILEY
N.G. GLUMAC✉

Laser-induced-fluorescence detection of SnO in low-pressure particle-synthesis flames

Mechanical and Industrial Engineering Department, University of Illinois, Urbana-Champaign, 1206 West Green Street, Urbana, Illinois 61801, USA

Received: 3 March 2003/Revised version: 16 June 2003
Published online: 10 September 2003 •

ABSTRACT Ground-state SnO has been observed in a flame for the first time using laser-induced fluorescence. The (18-0) band of the $E^1\Sigma^+ - X^1\Sigma^+$ transition is used for excitation. SnO is found to rapidly predissociate after excitation, and the tin atom emerges electronically excited, generating a fluorescence spectrum of atomic tin lines. This transition is found to be strong enough to excite in the linear regime, and the discrete nature of the fluorescence spectrum facilitates detection in environments with strong scattering and other interferences. However, quantitative analysis is hindered by a high density of SnO lines due to the many tin isotopes. Spatial SnO profiles in a hydrogen/oxygen/tetra-*n*-butyltin flame are obtained using this technique, and these profiles are qualitatively similar to metal monoxide profiles in other oxide-synthesis flames.

PACS 42.62.Fi; 33.50.Dq; 81.20.Ka

1 Introduction

Gas-phase tin monoxide (SnO) has received considerable attention in previous studies due to its potential for use in high-efficiency chemical lasers [1]. In addition, SnO appears as an intermediate in the combustion of tin-bearing species in air or oxygen, and SnO emission bands are readily observed in such flames (see e.g. Fig. 1). Recently, the combustion of tin-bearing compounds to produce ultra-fine particulates (nanopowders) has been an active area of research [2, 3]. Flame synthesis offers an attractive route to high-rate nanopowder synthesis [4, 5], and ultra-fine tin oxide powders have great potential in high-surface-area catalysis and gas-sensing applications. The need for process diagnostics in these flames has generated renewed attention on SnO as a potential species to monitor during powder synthesis. The appearance of SnO in a flame indicates the early stages of pyrolysis of the tin-bearing precursor. The disappearance of gas-phase SnO may be related to the formation of more stable oxide species (e.g. solid SnO or SnO_2) via condensation or polymerization steps. Thus, SnO profiles in tin oxide producing flames can be used to monitor the combustion process, serving as an input to process-control algorithms, or such profiles can be used as a sensitive test of particle-synthesis and/or gas-phase-chemistry models for the flame environment. Similar tests have been performed in flames using other metal monoxide species including FeO [6], SiO [7], and PbO [8]. It is therefore desirable to have a well-developed diagnostic for monitoring ground-state SnO in a flame environment. In addition, such a diagnostic needs to be robust enough to generate signals in a particle-laden environment with interferences such as broadband absorption and fluorescence and a large scattering intensity.

✉ Fax: +1-217/244-6534, E-mail: glumac@uiuc.edu

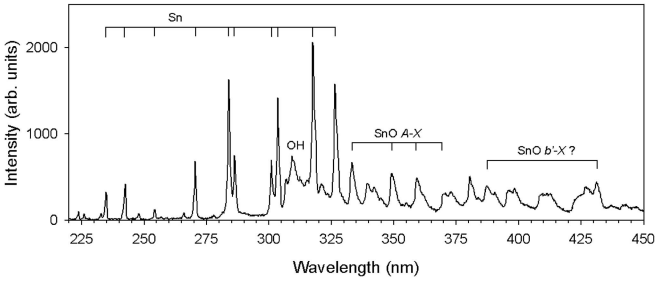

FIGURE 1 An emission spectrum from a low-pressure hydrogen/oxygen/tetra-*n*-butyltin flame showing features from Sn and SnO. The spectrum is not corrected for variations in detection efficiency

In this work we report the first detection of ground-state SnO in a flame environment. To perform this detection, we use laser-induced fluorescence (LIF), and we develop an excitation/collection strategy that is suitable for monitoring species in particle-laden flames. This work also represents the first LIF detection of SnO using the $E - X$ transition. Excitation of SnO is performed in the vicinity of 225 nm, a region which contains usable transitions for a large number of important combustion species. Therefore, this detection scheme can be readily incorporated into multi-species measurement strategies using a single laser scan.

2 SnO spectroscopy and previous work

The spectroscopy of SnO is well known as a result of several previous studies. Huber and Herzberg [9] summarize the details of the four of the five excited states of SnO accessible by visible or ultraviolet light. Capelle and Linton [1] suggest the presence of a fifth '*a*' state in the triplet system. A summary of the spectroscopic constants for the ground state and first five excited SnO states is shown in Table 1. Studies on the $E - X$ system by Appelblad et al. [10] and on the

State	T_e	ω_e	$\omega_e x_e$	B_e	Reference
$E^1\Sigma^+$	36298	505.01	2.70	0.27702	[10]
$A^1\Pi$	29625	587.6	2.5	0.3145	[10, 11]
$b'^3\Pi(1)$	24890	560	N.R.	0.2605	[9, 12]
$b^3\Pi(0^+)$	24333	555	N.R.	0.2964	[9]
$a^3\Sigma^+(1)$	20623	554	2.45	N.R.	[1]
$X^1\Sigma^+$	0	822.1	3.72	0.3557	[10]

TABLE 1 The ground state of SnO and the excited states accessible by visible or ultraviolet single-photon transitions. The units for all parameters are cm^{-1}. N.R. denotes 'not reported'

$A - X$ system by Clyne and Heaven [11] and Cheng-zai and Clyne [12] have most recently refined the constants for the X, A, and E states.

Most previous studies have used absorption or emission spectroscopy and have detected SnO without major difficulty due to the ease of generating large amounts of gas-phase SnO (e.g. as vapor pressure from solid SnO), as well as generally large transition strengths for many of the transitions in the visible and ultraviolet. However, spectroscopic studies of SnO are often complicated by the presence of 10 naturally occurring tin isotopes, seven with mole fractions in excess of 4%, leading to a high density of lines in the observed bands when using natural tin in SnO. Thus, some previous works have used SnO made from single isotopes of tin. SnO has been observed using fluorescence only by Clyne and Heaven [11] and Cheng-zai and Clyne [12]. Both studies investigated the $A - X$ transition, though the former study also included data from one band of the $b' - X$ transition.

The $E - X$ transition has been studied by a number of investigators, most recently by Appelblad et al. [10] who provided estimates of the spectroscopic constants of $^{120}Sn^{16}O$ based on an investigation of the bands with $v' = 1 - 11$ and $v'' = 0$, 1, and/or 2. Bands with $v' > 11$ have been observed at low resolution by Eisler and Barrow [13] who measured bands with v' as high as 18. The band furthest to the blue that was observed in that study was the (18-0) band, which is investigated in our work. The authors noted that there was a sharp drop in the vibrational interval starting at $v' = 18$, suggesting that this state was near the dissociation limit.

The (18-0) band of the $E - X$ transition of SnO is attractive from the perspective of combustion diagnostics since it is located in the 220–235 nm region where several other important combustion species, including NO [14], CO [15], O [16], O_2, and C_2H_2 [17], have accessible transitions for detection by LIF and/or absorption. Thus, if the (18-0) band has a sufficiently strong absorption cross section and fluorescence yield, SnO can be incorporated into multi-species detection schemes using a single absorption spectrum or a single excitation fluorescence scan.

3 Experimental apparatus

The experimental setup consists of a 30 cm diameter, 30 cm high vacuum combustion chamber with optical access. Inside the chamber, a 5 cm diameter flat-flame burner designed for particle synthesis generates a downward flow above a water-cooled substrate 2 cm below the burner face. The system typically operates at 20 Torr. Fuel and oxidizer enter the burner and are mixed with precursor vapors from liquid precursor that is added to a reservoir within the burner. An industrial band heater maintains the burner at an elevated temperature to generate the desired precursor vapor concentration in the flame as well as to minimize condensation of precursor vapors within the burner face. The precursor used in these studies is tetra-*n*-butyltin, which is an inexpensive metalorganic with low toxicity and thus is an excellent candidate precursor for large-scale industrial synthesis of tin oxide nanopowder. The fuel/oxidizer/precursor mixture generates a flame beneath the burner face, and product gases and powder impinge upon the cooled substrate. Flames such as this have been used extensively for oxide nanoparticle synthesis [18–24] and are very amenable to diagnostic evaluation for process-model validation [25].

For this study, the burner was a 5 cm diameter aluminum plate with an array of 1 mm holes on 2.5 mm centers. The substrate was water cooled and was 2 cm from the burner. The fuel was hydrogen and the oxidizer was oxygen. The total flow rate of fuel and oxidizer was 2 standard liters per minute, and the system pressure was 20 Torr. The precursor was maintained at either 164 or 155 °C. In the former case, the precursor mole fraction was estimated to be 0.002 ± 0.0005 based on measuring the weight of the precursor before and after the run. Using a scaling analysis based on the Clapyron equation, the mole fraction of precursor in the 155 °C case is estimated to be 0.0013.

Our fluorescence setup includes a Nd:YAG-pumped narrow-band dye laser (Continuum Jaguar) that uses Coumarin 450 dye. The fundamental output of the dye laser is frequency doubled with a BBO crystal to yield the requisite ultraviolet light in the neighborhood of 225 nm. The measured line width at 225 nm is 0.1 cm^{-1}, and the typical laser energy for these experiments is 100 μJ at 10 Hz, though measurable signal was obtained for powers down to less than 1 μJ/pulse. The laser is focussed into the chamber with a 250 mm focal length lens through a Brewster-angle window. A small portion of the inlet laser beam is split off and monitored by a photodiode for power correction. Fluorescence is collected at right angles to the incident beam using $f/3$ optics. Fluorescence is focussed on to the entrance slit of a 156 mm focal length monochromator (Jarrel–Ash Monospec 150) and is detected by a photomultiplier (Hamamatsu H3177-51) positioned behind the exit slit. The entrance and exit slit widths can be chosen for broadband detection of fluorescence (e.g. for maximum signal), or narrow-band (1 nm FWHM) detection to resolve fluorescence spectra by scanning the detection wavelength. The output of the photomultiplier is amplified and stored on a digital oscilloscope (LeCroy 9360). For excitation and fluorescence spectra, the gated fluorescence signal is averaged over 100 shots while, for spatial scans, the average fluorescence waveform is captured in order to extract fluorescence decay time information as well as amplitude.

4 SnO excitation spectra

Excitation spectra in the vicinity of the predicted (18-0) band were taken in 20 Torr flames. Fluorescence was typically collected in a 29 nm bandpass centered at 254 nm. This collection strategy offered good signal and

scattered laser light rejection. Excitation spectra are shown in Figs. 2 and 3. Eisler and Barrow [13] list the (18-0) band as degraded to the red with a head at 226.4 nm. At our higher resolution, there is no distinct band head, but the strongest lines do begin to appear in the band around 226.4 nm, though there are weaker lines observed out to at least 226.12 nm. The band does degrade to the red, and the density of the observed fluorescence lines is in agreement with our LIF model that considers the seven most abundant isotopes and uses spectroscopic constants from Appelblad et al. [10]. Furthermore, the spacing between the lines of the strongest branch (presumably the P branch of ^{120}SnO) is in good agreement with the model over two ranges that were investigated: 226.8 to 226.9 nm (model: 0.041 nm to 0.043 nm, experiment 0.037 ± 0.003 nm) and 228.0 to 228.2 nm (model: 0.069 nm to 0.070 nm, experiment: 0.069 ± 0.004 nm). Thus the band location, structure, line density, and spacing within a branch are in agreement with our assignment of this transition to the 18-0 band of SnO. This assignment is also supported by the observed fluorescence spectrum (see below).

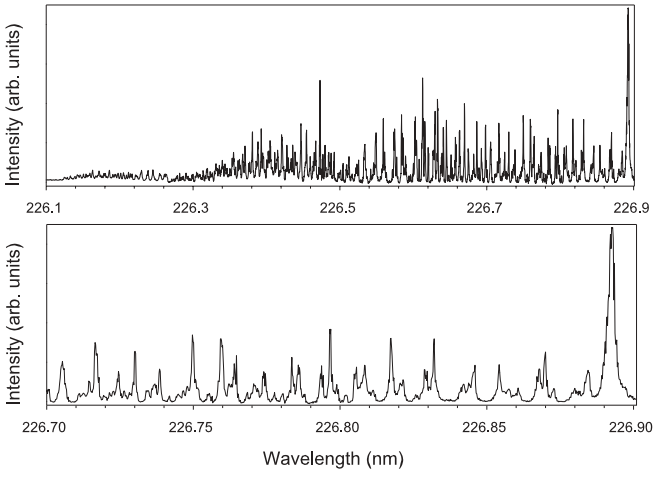

FIGURE 2 A LIF excitation spectrum of the (18-0) band of the $E - X$ transition in SnO in the vicinity of the band head. The *bottom plot* shows greater detail of the spectrum in the region 226.7–226.9 nm. The fluorescence was collected in a 29-nm bandpass centered at 254 nm

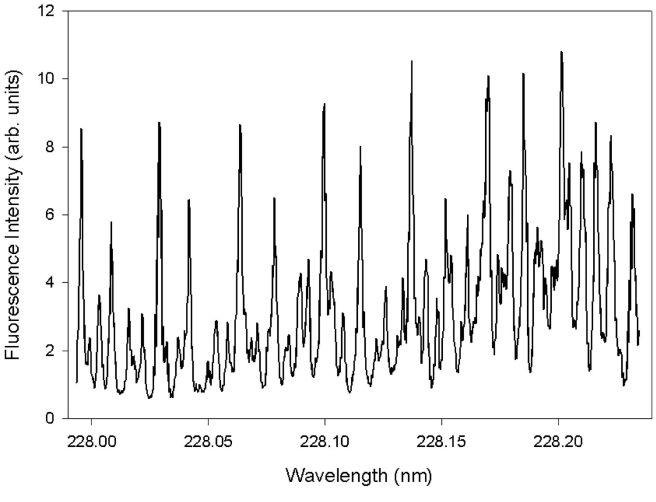

FIGURE 3 A LIF excitation spectrum in a region far removed from the band head. Simulations suggest that these lines should be P- and R-branch transitions with $J'' \approx 50$

The high line density of the fluorescence excitation spectrum, coupled with our level of resolution ($0.1\,\mathrm{cm}^{-1}$) generates an observed spectrum where most of the large peaks encompass two or more transitions. As such, line identification in this band is extremely difficult, and we have made no effort at identifying individual transitions.

A very strong feature in the excitation spectrum is observed at 226.891 nm and is assigned to an atomic tin transition. Though this transition does not involve the ground state of tin, the lower state ($^3P_2$) is only 3428 cm^{-1} above the ground $^3P_0$ state, and thus at our peak combustion temperatures up to 6% percent of the Sn atoms in the flame would be expected to be in the $^3P_2$ state. However, the bulk of the fluorescence intensity for this excitation wavelength is more likely due to excitation of tin atoms produced as a result of exciting overlapping SnO transitions that predissociate. This point is discussed further below. In either case, this line provides a suitable wavelength reference point, and thus we have used this line as our local wavelength calibration for the excitation scans.

Current spectroscopic constants for SnO suggest that the $v' = 19$ level of the excited E state in SnO is below the dissociation limit, and thus bands with $v' = 19$ may be observable, though none have been reported to date. The (19-1) band is predicted to have its origin in the middle of the (18-0) band, with lines of significant strength starting to appear at around 226.5 nm. Under our conditions, the $v'' = 1$ level is expected to have roughly half the population of the $v'' = 0$ level, which is easily enough population to detect. However, we did not see a significant increase in the density of lines anywhere near the expected band head. Thus, if the (19-1) band exists, then it is much weaker than the (18-0) band.

5 SnO fluorescence spectra

The observed fluorescence spectrum resulting from excitation of SnO lines in the (18-0) band is shown in Fig. 4. This spectrum does not change significantly with excitation wavelength. All the strong lines in the spectrum can be attributed to transitions of atomic tin. No transitions from SnO can be clearly identified. Based on this observation, it appears that the $v' = 18$ level of the E state rapidly predissociates into atomic O and electronically excited Sn. Transitions from several electronically excited Sn states are observed, and Table 2 provides a summary of these transitions. In general, it appears that the most commonly observed direct products of predissociation are the $5d\,^3D_3^\circ$, $5d\,^3D_2^\circ$, and $6s\,^3P_2^\circ$ states of tin. A second set of transitions is observed with a fluorescence decay profile that peaks at a time 10–20 ns after the laser pulse. These transitions involve primarily the $6s\,^3P_1^\circ$, $^3P_0^\circ$, and $^1P_1^\circ$ upper states, and the delay in fluorescence suggests that these states are not produced as a direct result of predissociation, but are rather generated as a result of collisional processes from other excited electronic states.

Figure 5 shows the excitation and fluorescence transitions that are observed in this work. States of Sn and SnO that are not observed in transitions are omitted, and it is notable that there are many more SnO and Sn states between 0 and

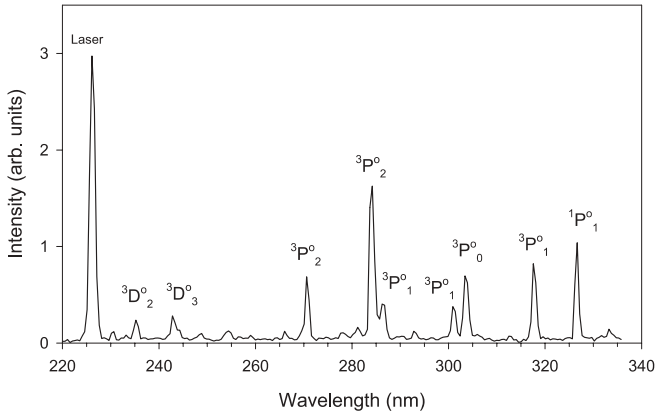

FIGURE 4 A fluorescence spectrum following excitation of the (18-0) band of SnO. These spectra are not corrected for relative system collection efficiency. All transitions are from excited atomic tin. Upper electronic states of atomic tin are listed above each transition. Full information of these transitions is given in Table 2

226.27 nm excitation – immediate fluorescence	
Wavelength (nm)	Transition
235.49	$5p^2\,{}^3P_1 \leftarrow 5d\,{}^3D^\circ_2$
242.95	$5p^2\,{}^3P_2 \leftarrow 5d\,{}^3D^\circ_3$
270.65	$5p^2\,{}^3P_1 \leftarrow 6s\,{}^3P^\circ_2$
284.00	$5p^2\,{}^3P_2 \leftarrow 6s\,{}^3P^\circ_2$
226.27 nm excitation – delayed fluorescence	
Wavelength (nm)	Transition
286.33	$5p^2\,{}^3P_0 \leftarrow 6s\,{}^3P^\circ_1$
300.91	$5p^2\,{}^3P_1 \leftarrow 6s\,{}^3P^\circ_1$
303.41	$5p^2\,{}^3P_1 \leftarrow 6s\,{}^3P^\circ_0$
317.50	$5p^2\,{}^3P_2 \leftarrow 6s\,{}^3P^\circ_1$
326.23	$5p^2\,{}^1D_2 \leftarrow 6s\,{}^1P^\circ_1$
226.89 nm excitation – additional lines	
Wavelength (nm)	Transition
219.93	$5p^2\,{}^3P_1 \leftarrow 5d\,{}^1D^\circ_2$
224.61	$5p^2\,{}^3P_0 \leftarrow 5d\,{}^3D^\circ_1$
257.16	$5p^2\,{}^1D_2 \leftarrow 5d\,{}^3F^\circ_3$
259.44	$5p^2\,{}^1D_2 \leftarrow 5d\,{}^1D^\circ_2$

TABLE 2 The atomic tin transitions observed in the fluorescence spectrum of the SnO molecule after (18-0) excitation in the $E - X$ band

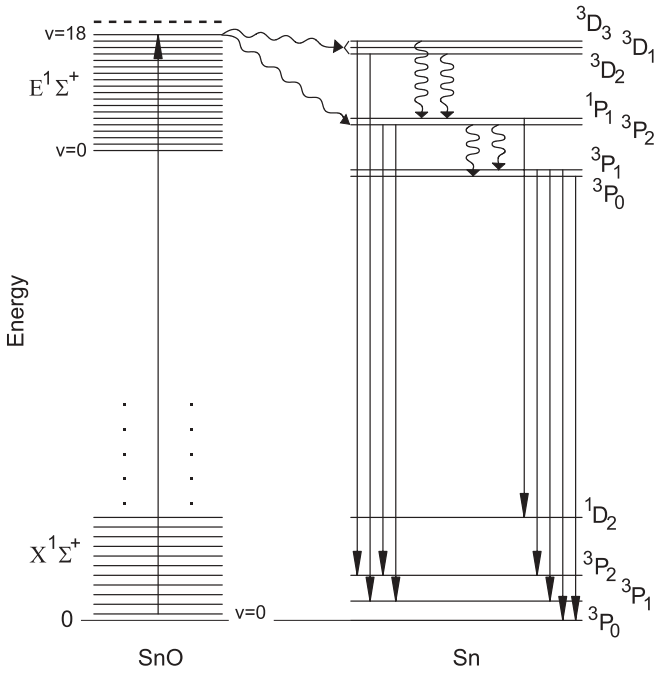

FIGURE 5 An energy-level diagram for our experimental approach showing radiative transitions (*straight lines*) and non-radiative transitions (*wavy lines*), including predissociation of the $v' = 18$ SnO E state and possible collisional routes to the upper states of Sn that are seen in delayed fluorescence. Note that since the dissociation products of the SnO E state are not explicitly known, the energy scales for Sn and SnO are not referenced to the same zero

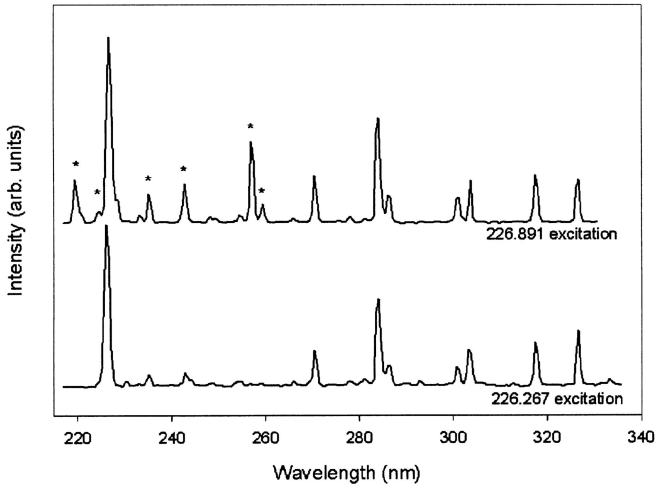

FIGURE 6 A comparison of the fluorescence spectrum of SnO obtained with excitation on and off the atomic tin line at 226.891 nm. New lines that appear and lines that appear stronger are shown with *asterisks*

50 000 cm^{-1} than are shown in the figure. The relative energy scales for Sn and SnO shown in the figure are not definitive, as it remains unclear as to what the dissociation products of the E and A states of SnO are [10]. However, based on our observation of atomic fluorescence following SnO excitation, we suggest that the products of dissociation of the E state are not the ground-state atoms, and the Sn must emerge in at least the ^3D or higher state.

Excitation exactly at the atomic tin line of 226.891 nm yields a similar fluorescence spectrum with three added lines, as shown in Fig. 6. Free tin atoms are likely present to some degree in flames such as these, though a detailed equilibrium analysis made using the multi-phase equilibrium code of Gordon and McBride [26] suggests that under these conditions the equilibrium gas-phase tin mole fraction should be several orders of magnitude lower than that of gas-phase SnO. The appearance of all the regular features in the fluorescence spectrum in roughly the same relative intensities suggests that the fluorescence signal at this wavelength, at least in significant measure, comes from excited Sn generated by SnO predissociation, rather than tin atoms naturally present in the flame. The three new transitions observed are from the closely spaced $5d\,{}^1D^\circ$, $^3D^\circ$, and $^3F^\circ$ states, the last of which is the directly excited upper state for the transition at 226.891 nm. Since the predissociation of SnO produces excited-state Sn that quickly decays to several low-lying states including the $5p^2\,{}^3P_2$ state, excitation of SnO by this LIF technique is a source of atoms that can then be excited (still during the laser pulse) by 226.891 nm radiation.

Thus, it is likely that the signal observed at 226.891 nm does not represent solely a measure of the local concentration of free atomic tin, but is also strongly linked to the local SnO concentration.

6 Flame-radical profiles

Despite the challenges in line identification, the (18-0) band can be used to obtain qualitative profiles of SnO in a flame environment. We used partially saturated LIF (pulse energies in the range of 10–100 μJ) with temporal resolution of the fluorescence signal to correct for quench-rate variation in the flame. The major uncertainty is in the correction for the Boltzmann fraction in the ground rotational state.

At low pressures such as these, mean times between collisions are typically significantly longer than the laser pulse (∼ 20 ns versus the 7 ns laser pulse), and thus collisional population and depopulation of the ground and upper states in the excited transition is insignificant during the laser pulse. Under these conditions, the peak fluorescence intensity is, to first order, proportional to the number density of the laser-excited state. Fluorescence decay after the peak is exponential with a time constant of $A + Q$, where A is the effective Einstein A coefficient for the upper state(s) excited by the laser and Q is the quench-rate coefficient and includes any collisional removal of population from the upper state of the transition that is monitored in fluorescence. The integrated area under the temporal fluorescence profile starting from the peak onwards is thus proportional to the peak intensity and inversely proportional to $A + Q$. The term $A + Q$ can be determined by fitting the decay of the temporal fluorescence profile to an exponential. In our experiments where fluorescence from a single upper Sn state is collected, collisional redistribution does not affect the result, and the decay is a good fit to a single exponential. Signal strengths could be significantly improved by monitoring a series of Sn transitions, but the decay would then not fit to a single exponential. Further studies are currently underway to optimize the collection strategy for optimum signal with minimal added uncertainty.

In our approach, we monitor the fluorescence waveform, measuring the area under the waveform and extracting the $A + Q$ value. The area divided by $A + Q$ is then used as a first-order estimate of the number density of the ground rotational state that is excited by the laser. A power correction for the variation of peak intensity with laser power is also made. The power-correction curve shows a strong, nearly linear, dependence of peak intensity on laser power, suggesting that the degree of saturation is small. We also correct for overlap of the beam and absorption line shapes using a $T^{1/2}$ correction, which should be good to first order for these systems where the laser line width is larger than the transition line width. Our approach does not explicitly account for collisional effects during the laser pulse or rotational energy transfer in the upper state after excitation. The former effect is small because of the long collision times, and the latter effect is likely negligible since all excited upper J states of $v' = 18$ rapidly predissociate. Beam-absorption effects were determined to be negligible in these flames by both absolute absorption measurements, which indicated a maximum of 1% non-resonant absorption from particles and gases at the highest precursor concentrations used, and by wavelength scans which showed less than 1% absorption by the strongest SnO lines.

The largest uncertainty in converting our fluorescence signal to a relative SnO number density is the Boltzmann fraction of the ground state in the laser-excited transition. We used a spectrum model based on the constants in the most recent study of the $E - X$ transition and constructed a predicted fluorescence spectrum. Though individual transitions are not reproduced in the model, the general band structure is a good fit. After shifting the location of the band head in the model to match the experiment, we isolated a region near the band head in the experimental spectrum in which there were strong isolated transitions. The model predicted that these transitions should be P- and R-branch transitions with J'' in the range of $12 - 18$. Based on this analysis we used a temperature correction based on $J'' = 15$. Since we are only concerned with relative number density profiles, we do not need to know the exact Boltzmann fraction, only the relative value as a function of temperature. Assuming that the line(s) that were excited fall in the range of $J'' = 10 - 20$, which we expect is a conservative estimate, the maximum systematic error from this correction over the expected temperature range (800–1600 K) is 5%. This uncertainty could, in principle, be verified by performing a series of spatial scans using different excitation wavelengths in this region of the spectrum. The temperature used in the correction is derived from an explicit 1-D flame model that has been shown to accurately predict the temperature profile in synthesis flames such as these [25]. Predicted temperature profiles for the two equivalence ratios used in this study are shown in Fig. 7. For the same flames as in this study, except for an added 15% diluent of 99% N_2, 1% NO, our earlier work showed good agreement between flame model predictions and NO rotational temperatures [27].

Precursor concentration in the flame increases with the vapor pressure of the liquid precursor, which is a strong function of temperature. Therefore, controlling the temperature is a means to similarly control the precursor concentration in the flame. Figure 8 shows two spatial SnO profiles taken at

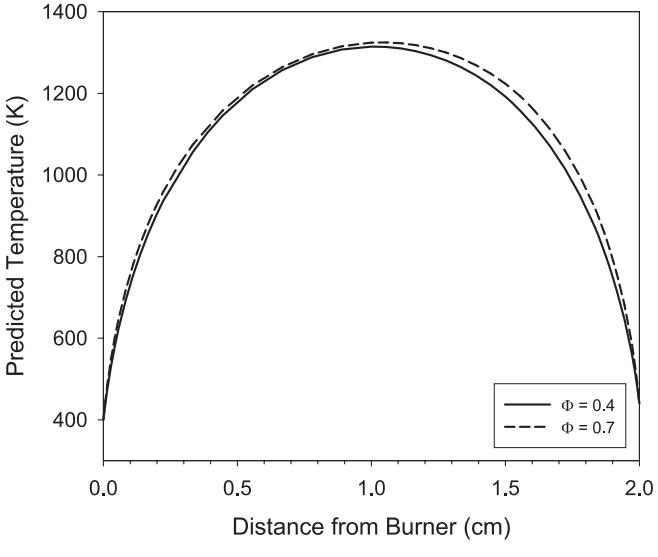

FIGURE 7 Predicted temperature profiles for H_2/O_2 flames at 20 Torr for the equivalence ratios of 0.4 and 0.7

slightly different precursor temperatures. At 150 °C, the powder production is just barely visible as a cloudy, white haze in the flame. Above 170 °C, the precursor concentration is too high for the flame to support in a stable fashion. Our two precursor temperatures, 155 and 164 °C, represent low and high precursor concentrations in the powder-producing range. As the precursor temperature is increased, the SnO number density increases, and the peak in the profile occurs closer to the burner. For both precursor concentrations, the SnO number density rises immediately in front of the burner and reaches a peak value before decaying as the flow approaches the substrate. In both cases, the SnO number density has dropped to less than a tenth of its peak value by 4 mm above the substrate.

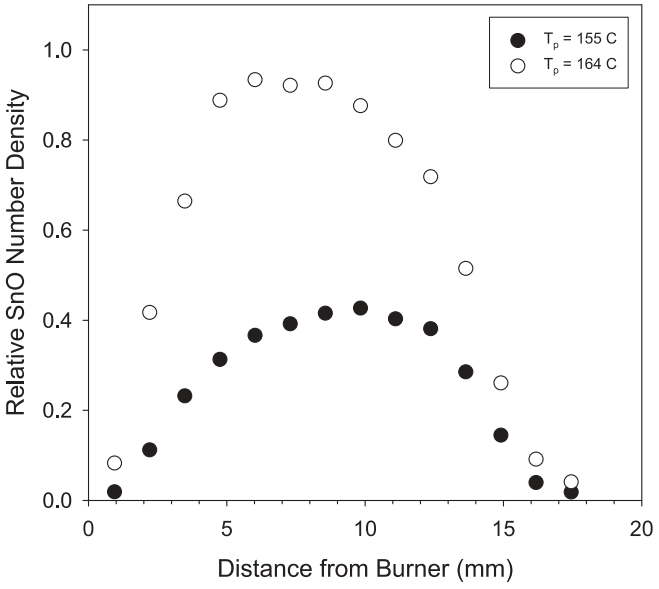

FIGURE 8 Spatial profiles obtained by LIF of relative SnO number density for two different precursor temperatures. For these two temperatures the precursor mole fractions were approximately 0.002 and 0.0013

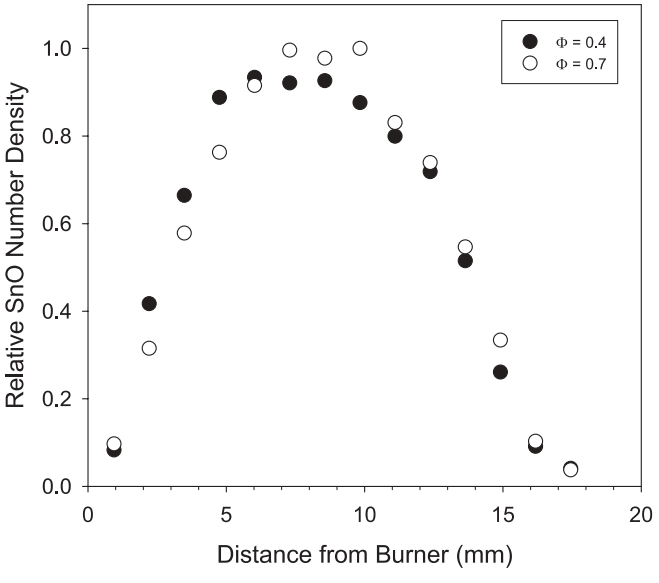

FIGURE 9 Spatial profiles obtained by LIF of relative SnO number density for two different overall flame equivalence ratios

The flame equivalence ratio can easily be varied independently of other parameters. For some monoxides, the observed number density in the flame is strongly dependent on the equivalence ratio while it is not for others [28]. We looked at two fuel-lean equivalence ratios of 0.4 and 0.75 at constant precursor temperature. For these two cases, the flame model predicted very similar flame temperatures with the 0.4 case having a peak temperature of 1315 K, and the 0.7 case a peak temperature of 1325 K. These results are shown in Fig. 9. The profiles are very similar in shape and magnitude, suggesting that there is not a strong equivalence ratio dependence on the SnO number density.

7 Discussion

Though there are several unusual aspects of our approach to investigating a flame intermediate by LIF, including the large Δv, the rapid predissociation of the excited state, and the high density of isotopic lines, the results suggest that this band is usable, at least in a qualitative sense, for diagnostic purposes. The excitation spectrum allows selection of a reasonable range of J'' to be excited such that the uncertainty in the relative profile is in the 5% range, which is adequate for many purposes. Collisional quenching effects, at least in these low-pressure flames, can be directly compensated for by using the explicit monitoring of the fluorescence decay profile. The measurements could potentially be made quantitative or semi-quantitative with the help of a heated calibration cell using solid SnO whereby the signal would be related to the partial pressure of the vapor phase. Temperatures of 1200 K would likely be sufficient based upon the heat of formation of SnO.

Since we do not know the absolute concentration of SnO in these flames, we cannot estimate a detection limit for this LIF strategy. However, compared to schemes used in similar flames, very low laser powers were required to obtain sufficient fluorescence signals. The power levels used are similar to those for SiO [7], OH [25], and NO [7], all of which can be observed in flames using linear fluorescence at powers of a few μJ per pulse. Species such as AlO and TiO required much higher pulse energies (closer to mJ levels [28]) to obtain a signal, even for flames with heavy precursor loading.

The fact that the fluorescence spectrum consists of tin lines may be of significant benefit in flame environments where many potential interferences exist. The fluorescence-collection scheme can incorporate a narrow-band filter or monochromator to isolate a single line or a pair of closely spaced lines, thus strongly rejecting broadband fluorescence and minimizing the chances of overlap from any other molecular fluorescence that is excited in the same region. Most of the profiles and spectra obtained in this study collected only one or two fluorescence lines, and signal strengths were more than adequate using collection optics with an f-number of 3.

The observed SnO profiles in these low-pressure flames are very similar to those seen in other studies of metal oxide producing flames, which further supports the validity of the chosen approach. Previous works looking at SiO [7], PbO [8], FeO [6], AlO, and TiO [28] have observed similar profiles with a sharp rise in number density near the burner and a peak in the profile that moves towards the burner as precursor concentration is increased. In addition, the early decay of SnO as

the flow approaches the substrate differs significantly from the decay region of the profiles of other flame radicals (e.g. OH), which persist in the flame much longer and are detectable to within a mm of the substrate. These SnO profiles are very similar to other metal monoxide profiles seen in analogous flames where SiO, AlO, and TiO were monitored. This early decay was analyzed in [7], and the conclusion was that such spatial profiles were indicative of a monoxide species that comes from two sources: as a product of precursor decomposition early in the flame, and as the partial pressure of the solid phase (here SnO and SnO_2) later in the flame. It was suggested that the partial-pressure effects dominate later in the flame and thus that the monoxide profile decays exponentially with the temperature as the flame gases cool on approaching the substrate. The strong similarity of the SnO profiles of this study with those of SiO from [7] suggests that similar phenomena control the monoxide profiles of both systems.

The small effect of flame equivalence ratio on the SnO profiles is similar to that seen in SiO and AlO, and in contrast to that seen in TiO. The slightly larger flame temperature for the richer flame should increase the peak mole fraction at the center of the gap region, but the higher temperature also reduces the number density. Since the former effect is exponential while the latter is linear, we expect the former effect to be dominant, leading to a slightly higher peak SnO number density at around the peak-temperature zone (i.e. near $z = 10$ mm), which is consistent with our observations. The leaner flame appears to oxidize the precursor slightly faster, leading to a quicker rise in SnO. This effect is consistent with a positive order for precursor decomposition with respect to oxygen concentration, which is also commonly seen in hydrocarbon systems.

8 Conclusions

Detection of ground-state SnO using LIF has been demonstrated in a powder-synthesis flame using excitation of the (18-0) band of the $E - X$ transition. The upper state is quickly predissociated to electronically excited tin and oxygen, leading to a fluorescence spectrum of atomic tin lines. Such a discrete spectrum offers considerable advantages in terms of rejection of interferences, which is important in particle-synthesis environments. Signal strengths for SnO are strong compared to other metal monoxides in similar flames, and linear excitation is possible in flames such as these. The qualitative SnO number density profiles obtained using (18-0) excitation in hydrogen/oxygen/tetra-*n*-butyltin flames are very similar to those of metal monoxides in the alumina, silica, and titania systems.

ACKNOWLEDGEMENTS This work was supported under an NSF CAREER award CTS-0096278 from the Combustion and Thermal Plasma Program.

REFERENCES

1 G.A. Capelle, C. Linton: J. Chem. Phys. **65**, 5361 (1977)
2 W. Zhu, S.E. Pratsinis: Ceram. Process. **43**, 2656 (1997)
3 D. Lindackers, C. Janzen, B. Rellinghaus, E.F. Wassermann, P. Roth: Nanostruct. Mater. **10**, 1247 (1998)
4 S.E. Pratsinis: Prog. Energy Combust. Sci. **24**, 197 (1998)
5 M.S. Wooldridge: Prog. Energy Combust. Sci. **24**, 63 (1998)
6 B.K. McMillin, P. Biswas, M.R. Zachariah: J. Mater. Res. **11**, 1552 (1996)
7 N.G. Glumac: Combust. Flame **124**, 702 (2001)
8 P. Biswas, M.R. Zachariah: Environ. Sci. Technol. **31**, 2455 (1997)
9 K. Huber, G. Herzberg: *Molecular Spectra and Molecular Structure, IV. Constants of Diatomic Molecules* (Van Nostrand Reinhold, New York 1979) p. 644
10 O. Appelblad, S. Fredin, A. Lagerqvist: Phys. Scr. **29**, 561 (1984)
11 M.A.A. Clyne, M.C. Heaven: Faraday Discuss. **71**, 213 (1981)
12 L. Cheng-zai, M.A.A. Clyne: Appl. Phys. B **44**, 99 (1987)
13 B. Eisler, R.F. Barrow: Proc. Phys. Soc. A **62**, 740 (1949)
14 D.E. Heard, J.B. Jeffries, G.P. Smith, D.R. Crosley: Combust. Flame **88**, 137 (1992)
15 M. Alden, S. Wallin, W. Wendt: Appl. Phys. B **33**, 205 (1984)
16 M. Alden, H.M. Hertz, S. Svanberg, S. Wallin: Appl. Opt. **23**, 3255 (1984)
17 B.A. Williams, J.W. Fleming: Appl. Phys. B **75**, 883 (2002)
18 Y.J. Chen, N.G. Glumac, G. Skandan, B.H. Kear: Mater. Lett. **34**, 148 (1998)
19 G. Skandan, Y.-J. Chen, N. Glumac, B. Kear: Nanostruct. Mater. **11**, 149 (1999)
20 Y. Chen, N. Glumac, B.H. Kear, G. Skandan: Nanostruct. Mater. **9**, 101 (1997)
21 D. Lindackers, M.G.D. Strecker, P. Roth: Nanostruct. Mater. **4**, 545 (1994)
22 D. Lindackers, M.G.D. Strecker, P. Roth, C. Janzen, S.E. Pratsinis: Combust. Sci. Technol. **123**, 287 (1997)
23 D. Lindackers, P. Roth: Ber. Bunsenges. Phys. Chem. **101**, 1718 (1997)
24 G.S. Tompa, G. Skandan, Y.-J. Chen, N. Glumac, B.H. Kear: Ceram. Bull. **78**, 70 (1999)
25 N.G. Glumac, Y.-J. Chen, G. Skandan: J. Mater. Res. **13**, 2572 (1998)
26 S. Gordon, B.J. McBride: NASA Ref. Publ. **1311**, 1 (1994)
27 S.N. Bailey, N.G. Glumac: In Proc. Eastern States Section Combustion Institute, Fall Meet., 2001, p. 296
28 A. Colibaba-Evulet, A. Singhal, N.G. Glumac: Combust. Sci. Technol. **157**, 129 (2000)